Measurement of the Roughness of the Sea Surface from Photographs of the Sun's Glitter

CHARLES COX AND WALTER MUNK
Scripps Institution of Oceanography, La Jolla, California*
(Received April 28, 1954)

A method is developed for interpreting the statistics of the sun's glitter on the sea surface in terms of the statistics of the slope distribution. The method consists of two principal phases: (1) of identifying, from geometric considerations, any point on the surface with the particular slope required for the reflection of the sun's rays toward the observer; and (2) of interpreting the average brightness of the sea surface in the vicinity of this point in terms of the frequency with which this particular slope occurs. The computation of the probability of large (and infrequent) slopes is limited by the disappearance of the glitter into a background consisting of (1) the sunlight scattered from particles beneath the sea surface, and (2) the skylight reflected by the sea surface.

The method has been applied to aerial photographs taken under carefully chosen conditions in the Hawaiian area. Winds were measured from a vessel at the time and place of the aerial photographs, and cover a range from 1 to 14 m sec^{-1}. The effect of surface slicks, laid by the vessel, are included in the study. A two-dimensional Gram-Charlier series is fitted to the data. As a first approximation the distribution is Gaussian and isotropic with respect to direction. The mean square slope (regardless of direction) increases linearly with the wind speed, reaching a value of $(\tan 16°)^2$ for a wind speed of 14 m sec^{-1}. The ratio of the up/downwind to the crosswind component of mean square slope varies from 1.0 to 1.9. There is some up/downwind skewness which increases with increasing wind speed. As a result the most probable slope at high winds is not zero but a few degrees, with the azimuth of ascent pointing downwind. The measured peakedness which is barely above the limit of observational error, is such as to make the probability of very large and very small slopes greater than Gaussian. The effect of oil slicks covering an area of one-quarter square mile is to reduce the mean square slopes by a factor of two or three, to eliminate skewness, but to leave peakedness unchanged.

1. INTRODUCTION

THE purpose of this study was to make quantitative measurements pertaining to the roughness of the sea surface; in particular, to learn something concerning the distribution of slope at various wind speeds. This distribution plays an important part in the reflection and refraction of acoustic and electromagnetic radiation, and in the complex problem of wind stress on the water surface.

Our method consists in photographing from a plane the sun's glitter pattern on the sea surface, and translating the statistics of the glitter into the statistics of the slope distribution. Winds were measured from a vessel at the time and place the photographs were taken. They ranged from 1 to 14 m sec^{-1}.

If the sea surface were absolutely calm, a single, mirror-like reflection of the sun would be seen at the *horizontal specular point*. In the usual case there are thousands of "dancing" highlights. At each highlight there must be a water facet, possibly quite small, which is so inclined as to reflect an incoming ray from the sun towards the observer. The farther the highlighted facet is from the horizontal specular point, the larger must be this inclination. The width of the glitter pattern is therefore an indication of the maximum slope of the sea surface.

Spooner[1] in a letter to Baron de Zach reports four measurements by this method in the Tyrrhenian Sea, all yielding maximum slopes of 25°. Hulbert[2] demonstrates by this method that the maximum slope in the North Atlantic increased from 15° at a 3-knot wind to 25° at an 18-knot wind. Shuleikin[3] took a long series of measurements of the width of the "road to happiness" over the Black Sea (a Russian synonym for the glitter pattern from the setting sun), and deduced that slopes up to 30° were not uncommon.

These measurements of maximum slope, so widely separated in space and time, are reasonably consistent. They do depend, however, on the manner in which the outer boundary of the glitter pattern is selected. This selection is apparently influenced by the brightness of the light source relative to the sky, and by the sensitivity of the eye. For otherwise the moon's glitter would not appear narrower than the sun's glitter under otherwise identical conditions. We have avoided this difficulty by computing the distribution of slopes from the measured variation of *brightness within the glitter pattern* (rather than computing maximum slopes from the outer boundaries). Our method gives more information—and requires much more work.

The two principal phases are (1) to identify, from geometric considerations, a point on the sea surface (as it appears on the photographs) with the particular slope required at this point for the reflection of sunlight into the camera, and (2) interpret the average brightness of the sea surface (or darkening of the negative) at this point in terms of the frequency with which this particular slope occurs. By choosing many such points we derive the frequency distribution of slopes.

* Scripps Institution contribution No. 737. This work has been supported by the Geophysical Research Directorate of the Air Force Cambridge Research Center, AMC, under contract No. AF 19(122)-413.

[1] J. Spooner, Corresp. Astro. du Baron de Zach, 6 (1822).

[2] E. O. Hulbert, J. Opt. Soc. Am. 24, 35 (1934).

[3] V. V. Shuleikin, *Fizika Moria* (Physics of the Sea) (Izdatelstvo Akad. Nauk. U.S.S.R., Moscow, 1941).

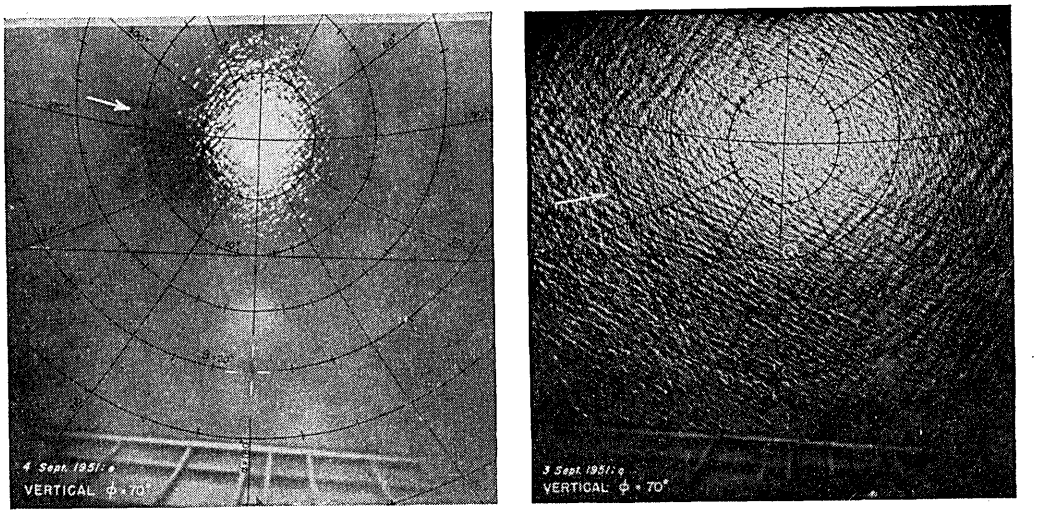

FIG. 1. Glitter patterns photographed by aerial camera pointing vertically downward at solar elevation of $\phi=70°$. The superimposed grids consist of lines of constant slope azimuth α (radial) drawn for every 30°, and of constant tilt β (closed) for every 5°. Grids have been translated and rotated to allow for roll, pitch, and yaw of plane. Shadow of plane can barely be seen along $\alpha=180°$ within white cross. White arrow shows wind direction. *Left:* water surface covered by natural slick, wind 1.8 m sec^{-1}, rms tilt $\sigma=0.0022$. *Right:* clean surface, wind 8.6 m sec^{-1}, $\sigma=0.045$. The vessel *Reverie* is within white circle.

2. THE OBSERVATIONS

Aerial Observations

The derivation of Sec. 4 will show that the radiance of reflected sunlight from the sea surface is determined by the probability distribution of slopes provided the light is reflected only once. To avoid multiple reflections we have made measurements only when the sun was high (only slopes greater than about one-half the angle of sun elevation can cause a second reflection). For a high sun the glitter pattern covers the surface to all sides of a point directly beneath the observer, and aerial observation is indicated.

A B-17G airplane was made available from the 3171st Electronics Research and Development Group, Griffiss Air Force Base, Rome, New York. Four K-17 (six-inch focal length) aerial cameras were mounted on a frame which could be lowered through the bomb bay and leveled during flight. They were wired for synchronous exposures. Two cameras pointed vertically downward, the other two pointed to port and were inclined downward at an angle of 30° with the horizontal. This allowed for a 25 percent overlap between the vertical and tilted photographs. One of the vertical cameras and one of the tilted cameras took ordinary in-focus or *image* photographs (see Fig. 1) using "variable density minus blue" filters. At an altitude of 2000 feet two points on the sea surface separated by more than 40 cm are resolved on the image photographs. The two remaining cameras took *photometric* photographs. From these cameras the lens systems had been removed, and glass sandwich filters containing Wratten gelatin A-25 absorbers installed.

During the photographic runs, the plane was steered by sun compass so that the azimuth of the tilted cameras was toward the sun. An attempt was made to avoid cloud shadows and atmospheric haze. In most cases the field of the cameras was sufficiently restricted to avoid these effects when the plane was flying at an altitude of 2000 feet.

Observations at Sea

In order to correlate measurements of wind speed with slope distribution free from modifying effects of land it was necessary to have meteorological records from a vessel near the location of the photographs. For this purpose a 58-foot schooner, the *Reverie*, was chartered and equipped with anemometers on the foremasthead (41 feet above sea level) and the bowsprit (9 feet). The signal from the anemometers was smoothed with an electrical low-pass filter having an 18-second time constant, then recorded. Wind direction was estimated by eye. Other measurements included the air and water temperatures, and the wet and dry bulb temperatures.

One of the objects of this investigation was to study the effect of surface slicks. First we attempted to spray powdered detergent from the vessel and later from the plane, but the slicks thus produced did not persist sufficiently. A satisfactory solution was to pump oil on the water, using a mixture consisting of 40 percent used crankcase oil, 40 percent Diesel oil, and 20 percent fish oil. With 200 gallons of this mixture a coherent slick 2000 feet by 200 feet could be laid in 25 minutes, provided the wind did not exceed 20 mph.

Location of Observations

During July, 1951, observations were taken offshore from Monterey, California, where a variety of wind

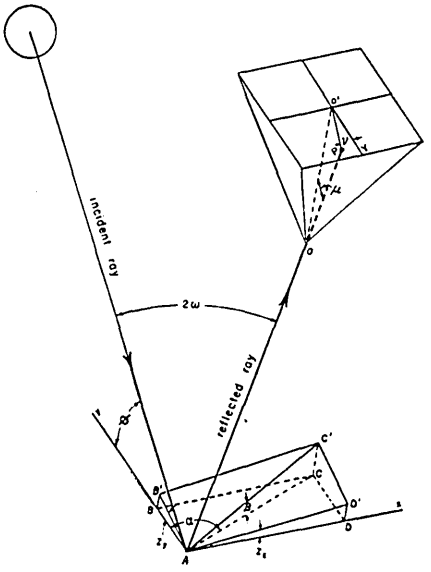

FIG. 2. The coordinate system is centered at the sea surface with the z-axis vertically upward (not shown) and the y-axis drawn horizontally toward the sun. The incident ray is reflected at A and forms an image at P on a horizontal photographic plate. Points A, B, C, and D define a horizontal plane through A and $AB'C'D'$, the plane tangent to the sea surface. The tilt β is measured in the direction AC of steepest ascent, and this direction makes an angle α to the right of the sun. OO' is parallel to the z-axis and $O'Y'$ to the (negative) y-axis.

conditions could be expected. Unfortunately the number of clear days was even smaller than given on climatological charts, and only two successful flights were completed.

By the end of July the sun elevation at noon was approaching our minimum requirement of 55° (to photograph plane's shadow; see Sec. 3), and it was decided to move the plane and vessel south to Hawaii. In this area one can select radically different wind conditions by moving short distances. The island of Maui was chosen because the region surrounding this island is the least clouded. Also, the harbor and airport facilities are conveniently near to one another. Conditions were excellent, and all observations were taken during the period August 25 to September 25, 1951.

3. THE GEOMETRY OF REFLECTION

The geometry of reflection has been considered by Minnaert[4] and Van Wieringen[5] with special emphasis on circular waves also by Hulbert[2] and by Eckart.[6] Here we shall require a systematic development which can be readily expanded into the second order calculations of the next section. The slope vector has the components (Fig. 2)

$$z_x=\partial z/\partial x=\sin\alpha\tan\beta,\quad z_y=\partial z/\partial y=\cos\alpha\tan\beta,\quad (1)$$

where α is the azimuth of ascent (clockwise from the sun) and β is the tilt.† A unit vector normal to the surface and positive upwards has the components

$$a_n=-\sin\alpha\sin\beta,\quad b_n=-\cos\alpha\sin\beta,\quad c_n=\cos\beta.$$

The unit vector along the incident ray has the components

$$a_i=0,\quad b_i=-\cos\phi,\quad c_i=-\sin\phi,$$

and along the reflected ray

$$a_r=-\sin\nu\sin\mu,\quad b_r=-\cos\nu\sin\mu,\quad c_r=\cos\mu.$$

According to the law of reflection the vector difference between the reflected and incident rays must lie along the surface normal:

$$\begin{aligned} a_r-a_i&=2a_n\cos\omega,\quad b_r-b_i=2b_n\cos\omega,\\ c_r-c_i&=2c_n\cos\omega, \end{aligned}\quad (2)$$

where $2\cos\omega$ is the proportionality constant. Squaring, adding, and making use of $a^2+b^2+c^2=1$ gives

$$\cos\omega=\cos\beta\sin\phi-\cos\alpha\sin\beta\cos\phi.\quad (3)$$

It can be verified that ω is the angle of incidence or reflection (Fig. 1). Equations (2) now yield the "grid" relations‡

$$\begin{aligned} \cos\mu&=2\cos\beta\cos\omega-\sin\phi,\\ \cot\nu&=\cot\alpha-\tfrac{1}{2}\csc\alpha\csc\beta\sec\omega\cos\phi. \end{aligned}\quad (4)$$

For any chosen orientation of the camera the angles μ, ν can be readily converted to film coordinates, and lines of constant α and β constructed (see Fig. 1). The grids are independent of the height of the camera, but depend on the solar elevation ϕ. The effect of the setting sun is to concentrate the pattern along a narrow street.

All photographs have been corrected for the roll, pitch, and yaw of the plane. With some care in flying, these angles can all be kept to within a few degrees. The correction then consists of a translation of the grid in order that the horizontal specular point on the grid coincides with that on the photograph, and a rotation so that the line $\alpha=0$ points toward the sun. The translation and rotation are uniquely determined from the positions on the photographs of the plane's shadow (clearest on Fig. 1, upper left) and of the horizon, allowance having been made for the depression of the horizon due to the earth's curvature. The formulas can be found in Sec. (3.1) of Cox and Munk.[7]

[4] M. Minnaert, Physica 9, 925 (1942).

[5] J. S. Van Wieringen, Proc. Koninkl. Ned. Akad. Wetenschap. 50, 952 (1947).

[6] Carl Eckart, The sea surface and its effect on the reflection of sound and light. University of Calif. Div. of War Research No. M407, March 20, 1946 (unpublished). The horizontal extent of the glitter pattern is assumed small compared to the distance from the observer.

† In geologic literature the attitude of a surface is described by its dip and strike. The former equals numerically the inclination angle β; the latter is measured 90° to the left (looking uphill) of α.

‡ In terms of other parameters the grid relations can become surprisingly complicated. In fact, Shuleikin (reference 3) considered the computation of such grids as "incommodious" and constructed them experimentally by projecting onto a screen the reflection from mirrors of constant slope.

[7] C. Cox and W. H. Munk, Scripps Inst. of Oceanogr. Bull. (to be published).

4. SURFACE RADIANCE

Up to now we have considered ordinary "in focus" photographs, or *image photographs*. These photographs show the presence of whitecaps, slicks, and cloud shadows. They also provide the basis for correcting for the roll, pitch, and yaw of the plane. Simultaneously with the tilted and vertical image photographs, and covering the identical fields of view, we have photographed the sea surface with two additional cameras from which lenses had been removed. The resulting out-of-focus photographs, or *photometric photographs*, provide the basis for computing frequency distributions of slope.

At the horizontal specular point the sea surface is likely to be so bright as to be blinding to the eye, whereas at some distance from this point the surface is much darker. The principal reason for this variation is that the gentle slopes (which are required for highlights near the horizontal specular point) occur more frequently than the steep slopes. On the *photometric photographs* the glitter pattern appears therefore as a round blob with a bright core (on the positive print), and gradually diminishing intensity to the outside. The density of the blob (on the negative) is then measured with a densitometer at points corresponding to the intersection of appropriate grid lines.

But there are other factors, in addition to the slope distribution, which help determine the density of the photograph. These are (1) the tolerance of slopes for the occurrence of a highlight at a fixed point, as related to the finite size of the sun; (2) the dependence of the coefficient of reflectivity of the water surface on the angle of incidence; (3) the ratio of sea surface area to the corresponding area on the photograph, for different points on the photograph; (4) the variable sensitivity of the camera to light from various directions; (5) the dependence of the film density on the exposure. These factors will now be considered.

4.1. The Tolerance Ellipse

Let the point z_{x0},z_{y0} on an z_x,z_y diagram (Fig. 3) represent the required slope at x_0,y_0 on the sea surface in order that a light beam from the sun's center striking this point be reflected into the camera. In order for x_0y_0 to be a highlight for a point source of light on the sun's periphery, the values z_{x0} and z_{y0} must vary by small quantities z_x' and z_y'. As the light source moves about the sun's periphery, it will trace an ellipse centered at z_{x0},z_{y0} on the z_x,z_y diagram. This ellipse defines a tolerance in possible values of z_x,z_y for a highlight at x_0,y_0.

It may be shown[7] that the area of the tolerance ellipse is

$$\Delta_t=\tfrac{1}{4}\pi\epsilon^2 \sec^3\beta_0 \sec\omega_0, \tag{5}$$

where $2\epsilon=32'.0$ is the angular diameter of the sun, and β_0,ω_0 the angles of tilt and incidence at the center of the highlight. The derivation assumes that the solid angle subtended by the highlight at the observer is small compared with $\pi\epsilon^2$, the solid angle subtended by the sun. This condition is always satisfied for an aerial observer.

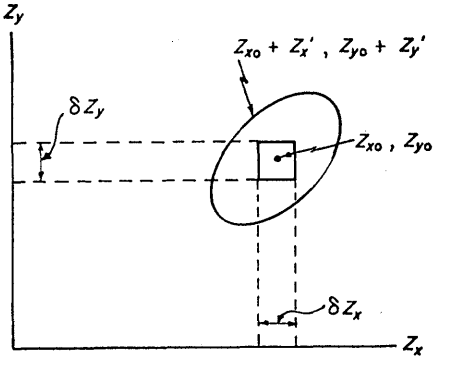

FIG. 3. The tolerance ellipse.

The tolerance ellipse relates the probability for the occurrence of a certain slope to the probability P for a highlight to occur in a certain area. Suppose we wish to find the probability $p(z_{x0},z_{y0})\delta z_x\delta z_y$ of slopes in the interval $z_{x0}\pm\frac{1}{2}\delta z_x$, $z_{y0}\pm\frac{1}{2}\delta z_y$ (Fig. 3). The probability of slopes occurring within the tolerance ellipse of area $\Delta_t(z_{x0},z_{y0})$ centered at z_{x0},z_{y0} equals

$$P(z_{x0},z_{y0})=p(z_{x0},z_{y0})\Delta_t(z_{x0},z_{y0}). \tag{6}$$

Thus if P can be measured, p can be readily computed.

The determination of P is a matter of some difficulty. One method would consist of recording the fraction of time, P, during which x_0,y_0 is a highlight, but this is difficult to accomplish from a plane. A measurement that comes closer to being feasible is the determination of the fraction of horizontal area in the immediate vicinity of x_0,y_0 that is highlighted during a very brief interval. This fraction is again equal to P, provided that in this vicinity all points have equal *a priori* probabilities of attaining a given slope. This provision excludes the edge of slicks, or regions where winds change rapidly. The observer must be sufficiently high that the "vicinity" of x_0,y_0 includes an area larger in linear dimensions than the wavelength of the longest ocean swell present.

Yet not even the fractional area that is highlighted can be measured directly from the photographs. In the first place, the individual glitters are too small to be resolved on the aerial photographs; what appears as an isolated highlight is actually a cluster of several hundred tiny glitters, each perhaps a millimeter in diameter. In the second place, the photographic image of a cluster is, because of its high intensity, many times larger than the image that would be obtained with a perfect optical system.

However, by means of the out-of-focus, or density photographs we can determine the *average* radiance over an area which includes many clusters of highlights. But the required quantity is the fractional area that is highlighted. Fortunately, the radiance and the frac-

tional area are proportional, and the latter can be computed from the former. The required relationship is derived in the next section.

4.2. The Scattering Cross Section

Let Δ_h designate the area of a single highlight projected onto a horizontal plane; then $\Delta_h \sec\beta$ will be the actual area on the (sloping) sea surface, and $\Delta_h \sec\beta \cos\omega$ the projection onto a plane normal to the incident rays. Let δH be the irradiance at the sea surface from a small surface element on the sun. The incident flux upon the highlight from this element is $\delta H \Delta_h \sec\beta \cos\omega$. The reflected flux is $\rho(\omega)\delta H \Delta_h \sec\beta \cos\omega$, where ρ is the reflection coefficient; it is radiated into a solid angle $\pi\epsilon^2$, the solid angle subtended by the sun. This result follows by reciprocity, as we have already shown that a bundle of parallel rays from the camera to the periphery of the highlight will be reflected around the periphery of the sun. Hence the intensity of the reflected beam (in power per unit solid angle) equals $\rho(\omega)\Delta_h \delta H (\pi\epsilon^2)^{-1} \sec\beta \cos\omega$. Since the camera aperture lies within the solid angle $\pi\epsilon^2$ regardless of the location of the element on the sun's surface, we can sum surface elements and replace δH by H, so that

$$J = \rho(\omega)\Delta_h H (\pi\epsilon^2)^{-1} \sec\beta \cos\omega \qquad (7)$$

is the reflected radiant intensity from *one* highlight.§ From a horizontal unit area of sea surface containing many such highlights and yet sufficiently small so that α,β can be considered constant from highlight to highlight, the reflected radiant intensity is

$$N \cos\mu = PJ, \qquad (8)$$

since P represents the fraction of surface that is highlighted under the assumption previously stated. Combining (5) to (8) yields the desired relation

$$p = 4\rho^{-1}(\cos^4\beta) N \cos\mu / H. \qquad (9)$$

The quantity N is the radiance of the sea surface in the line of sight, and the ratio $N \cos\mu/H$ has been called by Eckart[8] the "scattering cross section for unit solid angle per unit area of sea surface."

4.3. The Reflection Coefficient

The reflection coefficient $\rho(\omega)$ for unpolarized light at a dielectric interface is given by Fresnel's formula

$$2\rho(\omega) = \sin^2(\omega-\omega')\csc^2(\omega+\omega') + \tan^2(\omega-\omega')\cot^2(\omega+\omega'), \qquad (10)$$

where $\sin\omega = m \sin\omega'$ and m is the ratio of indices of refraction across the interface. For uncontaminated sea water $m = 1.338$, yielding $\rho(\omega) = 0.020$, 0.021, 0.060 and 1.00 for $\omega = 0°$, 30°, 60°, and 90°.

In the presence of slicks (Fig. 1, left) these values have to be somewhat modified. The artificial slicks laid by the boat consisted of a mixture of crankcase oil, sardine oil, and kerosene. The reflection at normal incidence is $\rho(0) = (m-1)^2/(m+1)^2$. For orientation, we consider monodecane with the refractive index 1.42. This gives $\rho_1(0) = 0.030$ for air-monodecane, and $\rho_2(0) = 0.001$ for the monodecane-water interface.

It is found that the thickness of the artificial slicks was of the order of several wavelengths of light, and about a thousand times the thickness of a monomolecular layer. By assuming that both faces of the oil layer reflect light according to Fresnel's law, the complete reflection coefficient (taking into account multiple reflections but disregarding interference effects) equals $\rho_1 + \rho_2(1-\rho_1)^2(1-\rho_1\rho_2)^{-1}$ for normal incidence. This gives 0.031 for monodecane, as compared to 0.020 for an uncontaminated water surface. The computed increase in reflectivity is in general agreement with the observed increase over artificial slicks.

Natural slicks are probably much thinner, perhaps only a few molecules thick.|| The effect on the reflection of light should then be negligible, and Eq. (10) should apply with $m = 1.338$. This has been confirmed by photometric measurements at normal incidence.

4.4 Photographic Photometry

The remaining problem is to relate the sea surface radiance $N \cos\mu$ to the film density D. There are some difficulties in the use of aerial cameras for photometry.

The photometric cameras were provided with red glass filters, and had a camera aperture of 1.7 cm. A point source (or any highlight) then has a nearly circular image with a diameter of about 1.7 cm. This size fulfills the following conditions: (1) it is large compared to the average distance between highlights, so that the highlights blend into one another and the grayness of the negative is not too spotty; (2) it is large compared to the size of the measuring aperture of the densitometer; (3) it is not large compared to the grid interval between isoclines and isogons.

Suppose s is the distance from the highlighted area (OA in Fig. 2), d is the diameter of the aperture, and λ the angle between the principal axis of the camera and the reflected ray [$\lambda = \mu$ for an exactly vertical camera (Fig. 2)]. The solid angle subtended by the aperture is $\frac{1}{4}\pi d^2 s^{-2} \cos\lambda$. Then since $N \cos\mu$ is the flux of radiation from a unit sea surface into a unit solid angle, $\frac{1}{4}\pi d^2 s^{-2} \tau(\lambda) N \cos\lambda \cos\mu$ is the corresponding flux into the photosensitive emulsion.

The transmission $\tau(\lambda)$ allows for (1) the reflection of the incoming rays by the outer face of a filter; (2) by the inner face; (3) absorption of flux in the filter;

§ This result follows also from the general theorem that the incident and reflected powers per unit area per unit solid angle are equal for a perfect reflector.

[8] C. Eckart, J. Acoust. Soc. Am. 25, 566 (1953). Here the linearized equations are developed for the case where the incoming radiation is not necessarily short compared to the ocean waves. For the limiting case of short-wave radiation, Eckart obtains essentially $p = 4\rho^{-1}(N \cos\mu/H)$.

|| Preliminary measurements by Kittredge indicate monomolecular slicks.

(4) reflection by the gelatin on the photographic plate; and (5) the vignetting effect resulting from the finite width of the aperture. The index of refraction of glass and the gelatin is 1.52, and hence each of the effects (1), (2), and (4) is proportional to $1-\rho(\lambda)$, where $\rho(\lambda)$ is Fresnel reflectivity, Eq. (10). Altogether the intensity is therefore reduced by a factor $[1-\rho(\lambda)]^3$.

The absorption of energy by the red filter consists first of a constant term involving the absorption of solar power for wavelengths less than 580 mμ. Of the energy in the band 580 mμ to 660 mμ, 20 percent is absorbed in the case of normal incidence and 24 percent for a ray traveling obliquely through the filter to the corner of the photograph. Wavelengths greater than 660 mμ are unimportant since the film is not sensitive to them.

The vignetting effect was computed from the dimensions of the aperture. The computation was checked by measuring the deviation from a circle of an image formed by a point source. All of these effects combined result in a ratio $\tau(45°)/\tau(0°)=0.81$ between the transmission at the extreme corner of the photograph and that at the center.

The product (flux) (exposure time) gives the luminescent energy reaching a unit film area during the entire exposure from a unit area of sea surface. Altogether this unit area of film receives energy from Δ_u unit areas of sea surface amounting to

$$E=\tfrac{1}{4}\pi d^2 s^{-2}\tau(\lambda)t\Delta_u \cos\lambda \cos\mu \qquad (11)$$

units of luminescent energy in an exposure of duration t. It can be shown that $\Delta_u=s^2f^{-2}\cos^3\lambda \sec\mu$, where f is focal length, and therefore

$$N=C \sec^4\lambda(\tau)^{-1}E(D),$$
$$C=(4f^2)/(\pi d^2 t). \qquad (12)$$

The photometric photographs were placed over the appropriate grids (translated and rotated to allow for roll, pitch, and yaw), and the intersections for every ten degrees of α and five degrees of β marked on the films. Additional intersections were marked for low winds and slick sea surface. The density D at each marked position was measured by a Welch "Densichron." The reproducibility of these measurements was ± 0.02 in density.

Additional measurements of density were made on each set of photometric photographs at corresponding points of the overlapping regions between the tilted and vertical films. Comparison of these pairs of densities was the basis of adjusting the calibrations for tilted and vertical films to common (but still arbitrary) units, and to remove any inconsistencies between the two calibrations.

The exposure $E(D)$ was determined from the density D of the film by comparison with the density produced by a light of known intensity. Because of the failure of the reciprocity law the calibration exposure had to be the same as the exposure on the flights. The calibration light source consisted of a concave diffusing surface (from a Federal 4-in.×5-in. cold light enlarger) illuminated by 39 incandescent bulbs arranged in a ring within the periphery of the diffusing surface. The calibrating light was passed through a Wratten A-25 filter in order to restrict the wavelength range to those of the photometric photographs. (Sunlight reflected from white blotting paper gave similar results.) Before falling on the photographic film the light source was intercepted by an optical wedge (a modified Eastman Kodak projection print scale) with eleven steps of differing transmission ranging from 100 to 3.7 percent. The range of light intensities (100 to 3.7) from a single calibration was extended by making several exposures with differing voltages on the incandescent lamps. Curves of D *versus* log$E$ were drawn for each exposure and fitted together by comparison of the overlapping range of densities. In this way a calibration range of light intensities of 1000 to 1 was obtained.

Calibrations were made before and after each flight. The roll film (super XX with 9-in.×9-in. negatives) was developed in motor-driven tanks using D-76 developer. On a roll containing only calibration exposures it was found that the slopes, γ, of the D-log$E$ curves varied by less than 3 percent except for exposures within 12 ft of the ends of the roll. Consequently leaders of this length were left on the ends of all photometric photograph rolls. Sets of calibration exposures were made at the beginning and end of each roll and at intervals within the roll so that there were never more than 15 photometric photographs between calibrations. Because of various malfunctions of the developing machines, the various calibrations on one roll gave values of γ varying by as much as 10 percent. The development of the photometric photographs was carried out to a γ of about 0.8. With this development the film was able to register light whose intensity varied over a range of more than 1000 to 1.

4.5. Relationship between Probability and Film Densities

Equation (9) expresses the slope probability p as a function of surface radiance N, and (12) relates N to the film density D. These are the desired relationships. For the special case of the sun overhead and the camera *exactly* vertical, $\phi=90°$, $\mu=\lambda=2\beta$, and $p\sim\cos^4\beta \sec^3\mu E$, or $p\sim(1+\mu^2+\cdots)E$ for the probability distribution of small slopes. This linear relation (to a first order) between probability and exposure indicates the inherent soundness of the present method.

5. BACKGROUND RADIATION

In addition to the reflection of the sun's rays from the sea surface, there are two other distinct sources of radiation: (1) the skylight reflected at the sea surface, and (2) the sunlight scattered by particles beneath the sea surface. These provide the "background" against which the sun's glitter is measured.

On calm days, the scattered sunlight and reflected skylight are of roughly equal intensity directly beneath the plane. In this region it is difficult to recognize the configuration of the sea surface outside of the glitter pattern for two reasons: (a) the scattered light is nearly independent of the presence of waves; and (b) the sky reflection shows little contrast on different sides of waves because the reflected parts of the sky dome are about equally bright and the coefficient of reflection varies little from that for normal incidence. The skylight predominates at greater distances. One qualitative indication of the scattered sunlight is the existence of the plane's shadow outside the limits of the glitter pattern (Fig. 2).

In this section, rough estimates are made of these two sources of background radiation. On the basis of these estimates correction factors are introduced. Fortunately the ratio of signal to background can be made fairly large by the use of a red filter, because sunlight is white while the skylight and scattered light is blue. Near the horizontal specular point the ratio varies from 500:1 on a smooth sea to 15:1 on a very rough sea. But in computing the probability of the large (and infrequent) slopes, our method is essentially limited by the disappearance of the glitter radiation into the background of the reflected skylight and scattered sunlight.

5.1. The Reflected Skylight

We consider the fraction $p(z_x,z_y)\delta z_x\delta z_y$ of a small (horizontal) unit area of sea surface for which the slope is within the limits $z_x\pm\frac{1}{2}\delta z_x$, $z_y\pm\frac{1}{2}\delta z_y$. The corresponding actual area within these limits is $\sec\beta p\delta z_x\delta z_y$, and the area projected normal to the line of sight is $\cos\omega\sec\beta p\delta z_x\delta z_y$.

Let the radiation incident onto the sea surface from the sky be characterized by its radiance N_s. The reflected radiance is $N_s\rho(\omega)$. We assume the light is reflected only once. Hence the radiant intensity at a great distance from this fractional part of the sea surface is $N_s\rho(\omega)\cos\omega\sec\beta p(z_x,z_y)\delta z_x\delta z_y$. The radiance due to all slopes is then

$$N'=\sec\mu\int\int N_s\rho(\omega)\cos\omega\sec\beta p(z_x,z_y)dz_xdz_y, \quad (13)$$

the limits of integration being such that all visible slopes are included. Equations (13) and (9) are the corresponding expressions for radiance due to skylight and sunlight.

The procedure for evaluating the integral is as follows: We anticipate (Sec. 6) that to a first order the slopes are normally distributed and independent of wind direction according to $p=(\pi\sigma^2)^{-1}\exp-(z_x^2+z_y^2)/\sigma^2$ where σ is the rms slope regardless of direction. As a rough approximation the sky dome is assumed uniform, $N_s=$constant. A rotated coordinate system is set up with the y' axis drawn in the direction of the small area of sea surface for which the radiance is sought. In this coordinate system

$$\cos\omega=\cos\beta(\cos\mu+z_y'\sin\mu).$$

Other terms in (13) remain unchanged. The quantities $F(\omega)=\rho(\omega)\cos\omega$ and $\sec\beta=(1+z_x'^2+z_y'^2)^{\frac{1}{2}}$ may now be expanded in Taylor's series in z_x',z_y' around the values $z_x'=z_y'=0$, for which $\beta=0$, $\omega=\mu$. This yields

$$N'=(\pi\sigma^2)^{-1}N_s\rho(\mu)\int\int(1+az_y'+bz_y'^2+cz_x'^2+\cdots)\times\exp[-(z_x'^2+z_y'^2)/\sigma^2]dz_x'dz_y', \quad (14)$$

where

$$a=-(F'/F),\quad b=\tfrac{1}{2}+\tfrac{1}{2}(F''/F),\quad c=\tfrac{1}{2}+\tfrac{1}{2}(F'/F)\cot\mu.$$

The functions F, $F'=dF/d\omega$ and $F''=d^2F/d\omega^2$ are evaluated at $\omega=\mu$.

If all slopes are less than $90°-\mu$, then the sea surface is everywhere visible, and the limits of integration are essentially $\pm\infty$. Large negative slopes in the component z_y' are not visible if they exceed $\cot\mu$ in magnitude. We shall allow for this "first-order" hiding by setting the limits $(-\cot\mu)$ to ∞ for z_y' (but $\pm\infty$ for z_x'). This is equivalent to the limits 0 to $\frac{1}{2}\pi$ in the angle of incidence ω. Because some additional slopes are hidden, the computed value of N' will be somewhat too large for large μ. But the evaluation of the "second-order" hiding involves information on the spectrum of ocean waves, and in the absence of such information we must restrict ourselves to the first-order hiding. The approximation will be adequate for large values of the dimensionless parameter

$$k=\sigma^{-1}\cot\mu. \quad (15)$$

The integration between the indicated limits yields

$$N'=N_s\rho(\mu)\{\tfrac{1}{2}[1+I(k)]+\tfrac{1}{2}\pi^{-\frac{1}{2}}a\sigma e^{-k^2}+\tfrac{1}{4}b\sigma^2[1+I(k)-2\pi^{-\frac{1}{2}}ke^{-k^2}]+\tfrac{1}{4}c\sigma^2[1+I(k)]+\cdots\}, \quad (16)$$

where

$$I(k)=2\pi^{-\frac{1}{2}}\int_0^k e^{-t^2}dt$$

is the error integral.

So far we have neglected multiple reflections. If in the case of the *final* reflection the incident ray comes from *beneath* the horizon, then certainly there must have been at least one preceding reflection. The condition for this "first-order" multiple reflection is that z_y' be negative and exceed $\frac{1}{2}\cot\mu(1-\tan^2\beta)$ in magnitude. The product of coefficients of reflection of all but the last reflection is unknown but must lie between zero and unity. In the latter extreme case multiple reflections would not alter the radiance, and Eq. (16) is correct as it stands. In the former extreme case, the limits of integration in (13) must be replaced by $-\frac{1}{2}\cot\mu(1-\tan^2\beta)<z_y'<\infty$. These can be replaced by the limits $-\infty<z_x'<\infty$, $-\frac{1}{2}\cot\mu<z_y'<\infty$ because of the heavy discrimination of the exponential factor in

the integrand against contributions from large β. The result of this integration is again Eq. (16) but with

$$k=(2\sigma)^{-1}\cot\mu \qquad (17)$$

in place of (15).

Figure 4 shows the radiance of the sea surface as bracketed by these two expressions. In Figs. 5 and 6 curves of $N'\cos\mu$ are plotted against some experimental values for a calm and a moderately rough sea, respectively. On the calm day the reflected skylight can account for only slightly more than half of the background intensity near $\mu=0$.

5.2. The Scattered Sunlight

The above discrepancy is assumed to be due to scattered light from within the water. Qualitative evidence for the importance of scattered sunlight is given by the appearance of the plane's shadow outside of the glitter. Within the shadow the background radiance is reduced because of the absence of backscattered light, whereas the reflected skylight is not appreciably diminished.

An empirical relationship for the scattered sunlight as a function of μ was obtained by subtracting from the total measured background that amount due to the reflected skylight (Fig. 5). Two particular photographs (3 Sept *j*, 4 Sept *e*, Fig. 1, left) were chosen because the glitter was the smallest on record, and there was adequate space on the photographs to measure the background outside the glitter. It is found that the scattered sunlight is strongest directly beneath the plane ($\mu=0$), and decreases with increasing μ more rapidly than $\cos\mu$ but less rapidly than $\cos^2\mu$. A comparison of the photographs for 3 Sept *j* and 4 Sept *e* shows that the scattered sunlight is proportional to irradiance of the sun, as might be expected.

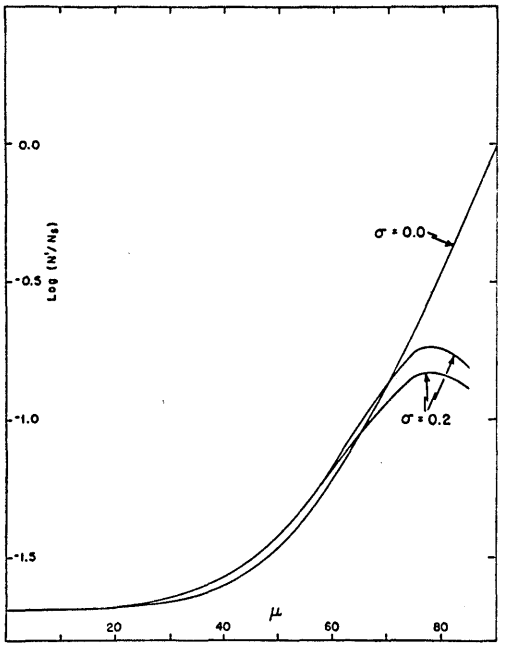

FIG. 4. The radiance (in arbitrary units) of a smooth sea surface ($\sigma=0$) and a rough sea surface ($\sigma=0.2$), according to Eq. (16). The two branches of the latter curve for large μ correspond to two extreme assumptions regarding multiple reflections.

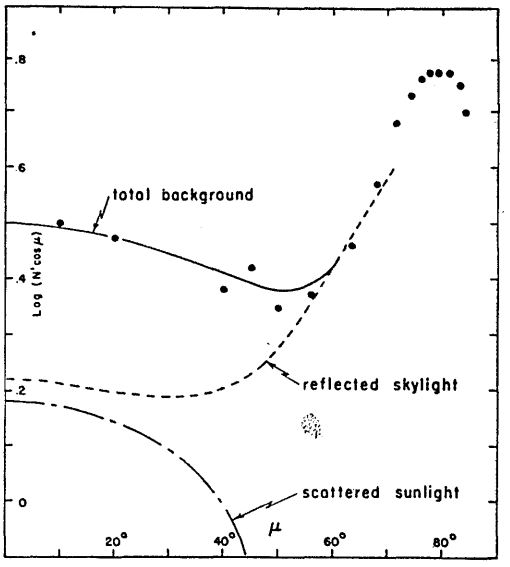

FIG. 5. The solid circles show the measured background on a very calm day (3 Sept *j*, $\sigma=0.091$), when the glitter pattern was confined to a small portion of the photograph. This background is due partly to reflected skylight, partly scattered sunlight, as shown.

5.3. Correction for Background

In the following procedure for allowing for skylight and scattered sunlight it will be assumed that the empirical law for the scattered sunlight is independent of the roughness of the sea surface, but depends only on the irradiance H from the sun. Measurements of the glitter (uncorrected for skylight) are used to determine σ and H to a first approximation. Using this value of H, the curve for the scattered sunlight is drawn (Fig. 6). Then measurements on the tilted photograph of skylight intensity from regions outside the glitter (Fig. 6, solid circles) are used to fix the sky intensity. By means of the curves of Fig. 4, sky reflection is extrapolated to $\mu=0$ using the appropriate value of σ. The curves for scattered sunlight and reflected skylight are then combined to give the total background as function of μ. Finally, this background is subtracted from the observed radiance.

On photographs taken at high wind speeds, the glitter pattern covers the entire field of view of both tilted and vertical cameras. Intensities from regions where the glitter reflection is weak give a basis for finding an upper limit to the background light. In all cases it has been found that the upper limit of the ratio of total background intensity to sun intensity varies by less than 30 percent. The indication then is that the upper limit of the background is not far in excess of the real background.

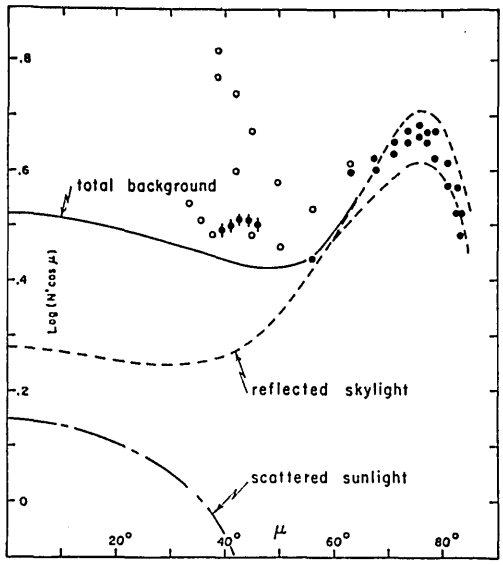

FIG. 6. The background radiation (in arbitrary units) on a moderately rough day (4 Sept k, $\sigma=0.13$). The solid circles correspond to measurements outside the glitter pattern. The open circles contain some glitter radiation, and lie, therefore, above the background curve. Circles with the vertical line correspond to measurements on the vertical photograph, the other circles to measurements on tilted photograph.

6. STATISTICS OF SLOPE DISTRIBUTION

The log of the unnormalized probability (corrected for background) at the various α,β-grid intersections has been tabulated for each set of photographs. A typical set of measurements—not the best—is shown in Fig. 7 and will be used as an example in the following discussion.

Rather than presenting tabulated values, it is more compact to present the results in analytical form as a function of wind speed, and thus bring out the essential physical content. In this way the experimental error is also subdued. A reasonable approach is to make use of the fact that the distribution is close to Gaussian. By representing the data as a Gram Charlier series we can develop the deviation from the normal distribution in a systematic manner. These deviations represent skewness and peakedness and therefore have a simple physical interpretation.

6.1. The Gram Charlier Series

The Gram Charlier distribution[9] in two dimensions assumes the form

$$p=[\text{two-dimensional Gaussian distribution}]\times[1+\sum_{i,j=1}^{\infty} c_{ij}H_i(\xi)H_j(\eta)].$$

The summation on the right represents the deviation from a normal distribution. It consists of products of Hermite polynomials H_iH_j with coefficients c_{ij} to be determined. The arguments ξ,η are defined below. The Gaussian distribution is represented in general by a product of three exponentials: two are functions of the two slope components separately and the third a function of their cross product. By a suitable rotation from the "sun x,y-system" it is always possible to suppress the cross-product term. This defines the principal axes, x',y'. As is to be expected, one of the principal axes is found to be parallel to the wind direction. The y' axis is arbitrarily defined to be this axis and to point upwind.

Some simplification of the summation term results from two empirical facts: (1) From many studies it is known that the mean slope is negligible over an area whose linear dimensions are much greater than the longest ocean wavelength. Hence $\langle z_x'\rangle_{Av}=\langle z_y'\rangle_{Av}=0$. (2) There is no asymmetry crosswind. This result follows from our own observations (Sec. 6.2).

A further simplification results by using the "standardized" slope components

$$\xi=z_x'/\sigma_c,\quad \eta=z_y'/\sigma_u,$$

where¶ σ_c and σ_u are the rms values of z_x' and z_y', respectively. The Gram Charlier distribution now assumes the form

$$\begin{aligned}p(z_x',z_y')=(2\pi\sigma_c\sigma_u)^{-1}\exp-\tfrac{1}{2}(\xi^2+\eta^2)\\ \times[1-\tfrac{1}{2}c_{21}(\xi^2-1)\eta-\tfrac{1}{6}c_{03}(\eta^3-3\eta)\\ +(1/24)c_{40}(\xi^4-6\xi^2+3)\\ +\tfrac{1}{4}c_{22}(\xi^2-1)(\eta^2-1)\\ +(1/24)c_{04}(\eta^4-6\eta^2+3)+\cdots].\end{aligned}\quad(18)$$

For slopes up to $\xi=\eta=2.5$ the present expansion is adequate. The rms slopes σ_c,σ_u, the skewness coefficients c_{21},c_{03}, and the peakedness coefficients c_{40},c_{22},c_{04} are to be evaluated from the data.

The procedure followed was to represent the data in the form of $\log p$, the *probability index*, as a Fourier series in α for fixed values of the tilt β. The amplitudes of the harmonic terms were then expressed as power series in the tilt. This permitted an analytic representation of the probability index for each photograph even where data were missing because of obscuring of glitter by whitecaps or slick patches. The connection between the power series coefficients and the rms slopes, and skewness and peakedness coefficients of Eq. (18) has been established[7] and in this indirect way the Gram Charlier series was fitted to the empirical data. Since the Gram Charlier series is normalized, no previous normalization of the probability was necessary.

6.2. Orientation of the Principal Axes

It will be seen from Fig. 7 that a Fourier analysis of the probability as a function of α (β=constant) will

[9] For example, Harald Cramer, *Mathematical Methods of Statistics* (Princeton University Press, Princeton, 1946). This gives a general account, but the development in two dimensions could not be found in the literature. Details are given in reference 7.

¶ The subscripts "c" and "u" refer to crosswind and upwind, respectively.

have a pronounced second harmonic. This feature has been used to rotate the x,y axes (the sun system) through an angle χ to the x',y' axes (the wind system) for which the probability distribution reduces to the form of Eq. (18). After fitting data to this form it was found (1) that the rotated y' axis points nearly into the direction of the wind** and (2) that the residuals (illustrated by the difference between the data points and the curves of Fig. 7) were reduced to "noise level."

The conclusions are (1) that the principal axes are in the direction of the wind and crosswind; (2) that there is no asymmetry crosswind. The observed wind direction and the empirical bearing of the positive y' axis (χ+sun azimuth) are summarized in Table I.

6.3. Mean Square Slopes

The mean square slope components, crosswind and up/downwind, were computed for each set of photographs (Table I). The two components, and the mean square slope $\sigma_c^2+\sigma_u^2$ (regardless of direction) vary nearly linearly with the wind speed W (in m sec^{-1}) recorded at 41 feet above sea level. The regression lines and correlation coefficients r have been computed by the method of least squares:

clean surface

$$\sigma_c^2 = 0.003+1.92\times10^{-3}W\pm0.002 \quad r=0.956$$
$$\sigma_u^2 = 0.000+3.16\times10^{-3}W\pm0.004 \quad r=0.945$$
$$\sigma_c^2+\sigma_u^2 = 0.003+5.12\times10^{-3}W\pm0.004 \quad r=0.986$$

slick surface

$$\sigma_c^2 = 0.003+0.84\times10^{-3}W\pm0.002 \quad r=0.78$$
$$\sigma_u^2 = 0.005+0.78\times10^{-3}W\pm0.002 \quad r=0.70$$
$$\sigma_c^2+\sigma_u^2 = 0.008+1.56\times10^{-3}W\pm0.004 \quad r=0.77$$

The ($\pm$) values give the standard deviations of the observed values from the corresponding values computed according to the regression lines. In computing the regression lines, each point is weighted according to the total number of densitometer readings on which it is based.††

6.4. Skewness and Peakedness

The determination of the skewness coefficients c_{21},c_{03} depends critically on the alignment of the grid and

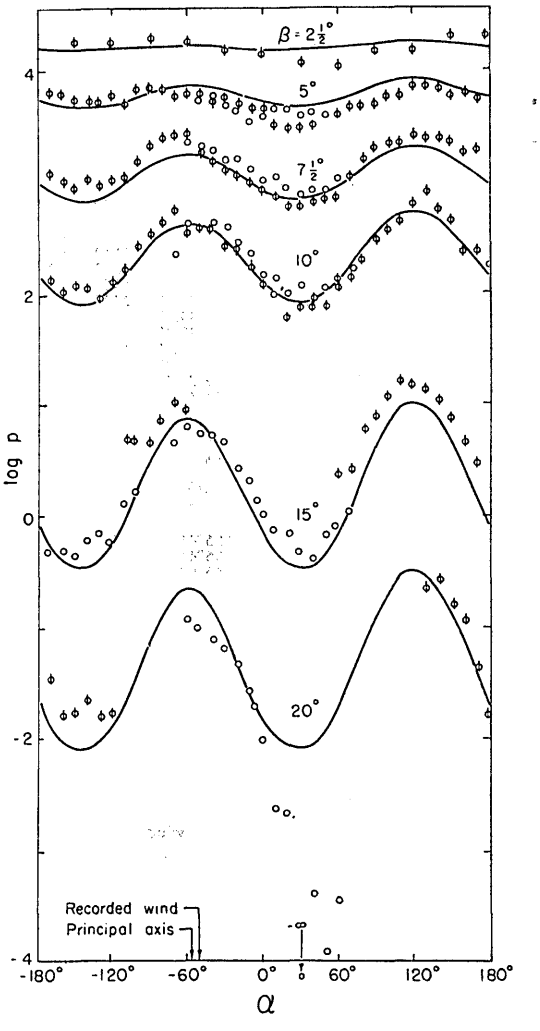

FIG. 7. Logarithm of unnormalized probability p as a function of azimuth α relative to sun, for indicated values of slope angle β. Open circles indicate data from tilted camera; barred circles, vertical camera. All measurements from photographs 4 Sept. k. Curves are drawn according to the Gram Charlier representation, Eq. (18). The position of the principal (y') axis is indicated relative to recorded wind direction.

photograph. The data show a rather large scatter, but apparently the magnitude of coefficients increases with increasing wind speed for uncontaminated water. The regression lines are

$$c_{21}=0.01-0.0086W\pm0.03$$

and

$$c_{03}=0.04-0.033W\pm0.12.$$

In the presence of slicks the scatter of points is too great to evaluate the dependence on wind speed, if any. The weighted mean values are

$$c_{21}=0.00\pm0.02 \quad \text{and} \quad c_{03}=0.02\pm0.05.$$

Within the accuracy of the measurements, the peakedness coefficients are independent of wind speed

** For nine photographic sets, 3 Sept. t; 4 Sept. y; 6 Sept. c; 10 Sept. k; 10 Sept. m; 10 Sept. r; 11 Sept. e; 11 Sept. f; and 13 Sept. e, the data showed no pronounced anisotropy. For these photographs the principal axes were arbitrarily taken in the direction of the wind and crosswind.

†† One point at $\sigma_c^2=0.0152$, $\sigma_u^2=0.0153$, $W=0.89$ m sec^{-1} (3 Sept t) was omitted in the calculation. The deviation of the $\sigma_c^2+\sigma_u^2$ value from the regression line is six times the standard deviation. Clearly some special conditions must apply to this observation. An examination of the wind record on 3 Sept. reveals that the wind was quite variable at the place where this observation was taken and was as high as 4.5 m sec^{-1} only 10 minutes before the photographs were taken. Quite possibly the wind speed at the vessel, which was just outside the glitter, was markedly lower than within the glitter area itself.

TABLE I.

Photograph designation[a]	Time[b]	Location of cameras N Lat	W Long	h (ft)[c]	Position of sun Altitude	Azimuth	Wind Speed (ms^{-1}) 41 ft[c]	9 ft[c]	Direction (true)	Sea surface	χ+sun az[d]	Mean square slope components σ_c^2	σ_u^2	Weight factor[e]
28 Aug *b*	1106	21°01.8′	156°45.8′	900	67°20′	119°	11.6	9.6	060°	clean	063°	0.0211	0.0390	125
28 Aug *p*	1336	20°59.0′	156°44.0′	2000	70°10′	236°	13.3	11.0	050°	clean	057°	0.0294	0.0484	155
28 Aug *u*	1403	20°58.2′	156°43.3′	2000	64°30′	246°	13.8	11.6	050°	clean	036°	0.0287	0.0452	157
28 Aug *v*	1403	20°58.2′	156°43.3′	2000	64°30′	246°	13.7	11.5	050°	clean	047°	0.0276	0.0404	160
3 Sept *j*	1157	20°39.5′	156°46.6′	2000	75°10′	150°	0.72	0.45	050°	clean	095°	0.00337	0.00489	114
3 Sept *q*	1330	20°39.5′	156°46.6′	2000	69°50′	230°	8.58	7.11	120°	clean	140°	0.0224	0.0230	158
3 Sept *l*	1357	20°39.5′	156°46.6′	2140	64°30′	242°	0.89	0.54	180°	clean	ε	0.0152	0.0153	181
4 Sept *e*	1126	20°40.2′	156°40.3′	2000	70°10′	131°	1.79	0.49	045°	Nat. slick	120°	0.00096	0.00126	84
4 Sept *k*	1158	20°39.0′	156°40.0′	1950	75°00′	152°	3.93	3.58	100°	clean	94°	0.00694	0.00977	179
4 Sept *n*	1257	20°39.5′	156°36.9′	2000	74°30′	209°	8.00	6.62	100°	clean	126°	0.0136	0.0191	182
4 Sept *r*	1324	20°40.0′	156°39.3′	2000	70°30′	228°	6.30	5.27	111°	clean	136°	0.0134	0.0170	136
4 Sept *v*	1327	20°40.0′	156°39.3′	1000	70°00′	230°	6.44	5.4	111°	clean	119°	0.0136	0.0186	137
4 Sept *y*	1353	20°39.5′	156°36.9′	1900	65°00′	241°	4.92	4.07	110°	clean	ε	0.0172	0.0174	139
5 Sept *b*	1058	20°40.5′	156°35.7′	1950	64°50′	121°	1.83	1.43	280°	clean	296°	0.00534	0.00906	156
5 Sept *g*	1124	20°40.1′	156°35.4′	1950	70°00′	131°	1.39	0.58	280°	clean	280°	0.00609	0.00875	156
5 Sept *j*	1354	20°46.8′	156°40.3′	2050	64°30′	240°	3.35	2.99	225°	clean	237°	0.0102	0.0125	188
6 Sept *c*	1048	20°58.5′	156°45.3′	1000	62°40′	120°	10.8	9.12	045°	clean	ε	0.0252	0.0265	42
										oil slick		0.0111	0.0108	73
6 Sept *k*	1124	20°58.0′	156°44.5′	2000	69°10′	135°	10.2	8.85	045°	clean	040°	0.0254	0.0357	159
6 Sept *q*	1237	20°57.5′	156°44.0′	2000	75°20′	195°	11.7	9.92	045°	clean	045°	0.0254	0.0374	151
10 Sept *k*	1328	20°40.0′	156°38.3′	1800	67°50′	225°	8.45	7.24	130°	oil slick		0.0102	0.0117	97
10 Sept *m*	1333	20°40.0′	156°38.3′	900	67°00′	228°	7.15	6.00	130°	oil slick	ε	0.00860	0.0100	100
10 Sept *r*	1347	20°39.7′	156°39.3′	2000	64°20′	232°	5.32	4.47	120°	clean	ε	0.0137	0.0179	59
										oil slick		0.00967	0.00985	67
11 Sept *e*	1317	20°45.5′	156°41.8′	1000	69°20′	220°	5.45	3.75	210°	clean	ε	0.0136	0.0137	137
11 Sept *f*	1317	20°45.5′	156°41.8′	1000	69°20′	220°	5.45	3.75	210°	oil slick	ε	0.0107	0.0109	108
13 Sept *e*	1308	20°17.6′	156°02.4′	2150	69°50′	215°	2.41	1.97	090°	oil slick		0.00391	0.00467	86
13 Sept *f*	1308	20°17.6′	156°02.4′	2150	69°50′	216°	2.41	1.97	090°	oil slick	076°	0.00724	0.00959	136
17 Sept *e*	1136	20°29.9′	156°24.8′	2000	68°40′	149°	9.79	8.31	086°[h]	clean	080°	0.0209	0.0264	79
										oil slick		0.0106	0.0126	45
17 Sept *c, h, k, n, q*[f]	{1111 1205	20°28′	156°24′	2000	{65°15′ 71°30′	{136° 169°	9.74	8.18	088°[h]	clean	087°	0.0230	0.0322	752
17 Sept *A*	1424	20°17.6′	156°14.8′	1800	54°40′	243°	10.5	8.45	068°[h]	clean	069°	0.0224	0.0365	172

[a] Includes date of observation, 1951.
[b] Time meridian 150°W.
[c] Elevation above sea level.
[d] True azimuth of principal (y') axis.
[e] Number of densitometer readings contributing to probability distribution.
[f] Probability distribution derived from 5 photographic sets.
[g] Observed wind direction used.
[h] Wind direction estimated from direction of wind streaks on water; recorded wind direction appears to be in error by twice magnetic variation.

and have the values

clean surface:

$$c_{40}=0.40\pm0.23 \quad c_{22}=0.12\pm0.06 \quad c_{04}=0.23\pm0.41$$

slick surface:

$$0.36\pm0.24 \qquad 0.10\pm0.05 \qquad 0.26\pm0.31$$

For details of the fitting procedure which lead to these values for the skewness and peakedness coefficients, as well as a tabulation of individual values of the probability index coefficients, we refer the interested reader to reference 7.

7. ESTIMATE OF ERRORS

In the preceding section we have included the standard deviations of the individual observation *from* the regression lines (for the mean square slopes and skewness) or *from* the mean values (for peakedness). The standard deviation *of* the mean peakedness is $n^{-\frac{1}{2}}$ times this value, where n is the number of observations. In addition, there are some systematic errors which do not show up in the scatter. A minor source of systematic error results from certain mathematical approximations in Sec. 6. These affect only skewness and peakedness.

Random Errors

Imperfections in the developing of the films result in errors in the photographic γ and these cause roughly proportional errors in the mean square slopes. They amount to about $\pm$ five percent. A more important source of error arises in the subtraction of background light. It will be recalled that the sky intensity curves were fitted to the reflected light just outside the glitter pattern (Sec. 5.3). This fitting is critically affected by the low intensity "toe" of the D-log$E$ calibration of the photographic film and also by cloud reflections and other unknown factors. This is probably the principal cause of the scatter in peakedness. Variation in wind speed may also introduce scatter. Imperfect control for roll, pitch, and yaw by a fraction of a degree will introduce an error in skewness of the order of the scatter in skewness. In cases where the glitter is partly in a slick and partly out of a slick, the principal source of error in the skewness results from an imperfect separation of the data into these two categories.

Shadows and Multiple Reflections

Cloud shadows can be allowed for to some extent from a study of the image photographs.

Two complicating circumstances which have not been considered are (1) the presence of steep valleys in the sea surface which are hidden from the direct view of the camera,[10] or from the rays of the sun, and (2) the

[10] This accounts for the fact that one rarely sees distant trees, dunes, or ships reflected in the sea. The reason, as pointed out by Minnaert [M. Minnaert, *Light and Colour in the Upper Air*

occurrence of multiple reflections. By neglecting these complications we introduce errors into any computation involving slopes steeper than one-half the elevation of the sun. We have largely avoided such errors by confining our measurements to sun elevations above 55°.

Whitecaps

At high wind speeds the problem of whitecaps requires special consideration. We have located the whitecaps on the image photographs, and have omitted the corresponding dark spots on the photometric photographs from our measurements. At high winds this is troublesome, and we are likely to overestimate the frequency of high slopes. For some purposes it may have been more useful to determine the slope distribution regardless of whether such slopes are or are not related to whitecaps. Our method is not capable of doing this because of multiple reflection of light from foam bubbles.

Skylight

The major source of systematic errors results from the assumption of a uniformly bright sky dome in the background correction (Sec. 5.1). Without a further study of the variation in skylight it is impossible to estimate errors arising from this assumption. For high sun it seems reasonable that any deviations from uniformity depend largely on angular distance from the sun. In this case the resulting errors in mean square slope and skewness are small, but it is not impossible that this systematic error may be largely responsible for the calculated values of peakedness.

8. DISCUSSION AND SUMMARY

The Gram Charlier distribution function (18) gives an adequate description of the measured probability density p of the slope components up to two and one-half times their rms value. There is no information on larger (and more infrequent) slopes because of the limitations imposed by background radiation. With $m=\tan\beta$ designating the slope regardless of direction, and α' the angle of ascent measured to the right of the wind, it follows that

$$p dz_x' dz_y', \quad m p d\alpha' dm, \quad \text{and} \quad p \tan\beta \sec^2\beta d\alpha' d\beta$$

are the probability densities of slope within the limits

$$z_x' \pm \tfrac{1}{2} dz_x', \quad z_y' \pm \tfrac{1}{2} dz_y'; \quad \alpha' \pm \tfrac{1}{2} d\alpha', \quad m \pm \tfrac{1}{2} dm;$$

and

$$\alpha' \pm \tfrac{1}{2} d\alpha', \quad \beta \pm \tfrac{1}{2} d\beta,$$

respectively.

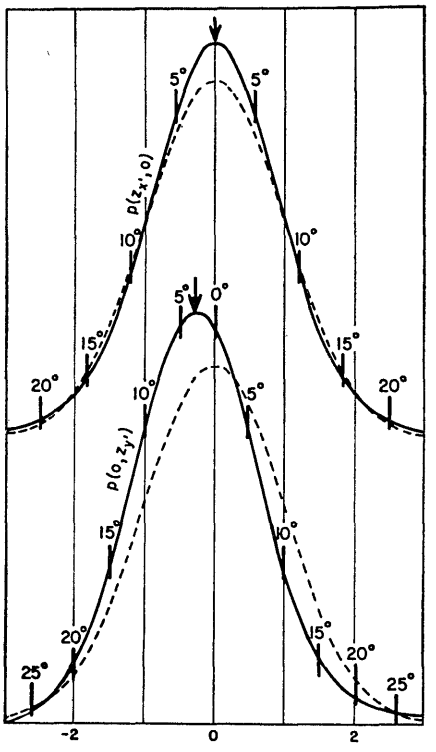

FIG. 8. Principal sections through the probability distribution surface $p(z_x', z_y')$. The upper curves are along the crosswind axis x'; the lower curves along the upwind axis y'. The solid curves refer to the observed distribution, the dashed to a Gaussian distribution of equal mean square slope components. The thin vertical lines show the scale for the standardized slope components $\xi = z_x'/\sigma_c$ and $\eta = z_y'/\sigma_u$. The heavy vertical segments show the corresponding tilts $\beta = 5°, 10°, \cdots, 25°$ for a wind speed of 10 m sec^{-1}; the skewness shown in the lower curve is computed for this wind speed. The modes are marked by arrows.

The distribution function p is illustrated in Fig. 8. The mean square slope regardless of direction, $\sigma_c^2+\sigma_u^2$, increases linearly with wind speed, reaching a value of $(\tan 15.9°)^2$ for a wind speed of 14 m sec^{-1} measured at 41 ft elevation. The crosswind component σ_c^2 and up/downwind component σ_u^2 each increase linearly with wind speed, but the correlation is poorer because the variability in wind direction affects them separately but not their sum.

The principal axes are found to be oriented with the wind. The up/downwind mean square slope components are somewhat larger than the crosswind components. The ratio σ_u^2/σ_c^2 varies from 1.0 to 1.8 with a mean value of 1.34 for all photographs. For the slick surface the mean value is 1.16. This large variability is far in excess of experimental error. It is probably the result of differences, from one case to the next, in the *variability* of the wind direction. Steady winds would lead to large values in σ_u^2/σ_c^2 whereas gusty winds would diminish this ratio to somewhere near unity.

The skewness coefficients c_{21} and c_{03} of the Gram Charlier series decrease with increasing wind speed

(G. Bell and Sons, London, 1940)], is that "at a great distance one sees only the sides of waves turned toward us. This makes it seem as if we saw all the objects . . . reflected in a slanting mirror." For the same reason, the reflection of low, distant clouds is displaced toward the horizon.

from nearly zero at very low winds to $c_{21}=-0.11$, $c_{03}=-0.42$ at 14 m sec^{-1}. At the higher wind speeds the most probable azimuth of ascent for low slopes is directed downwind, whereas for very large slopes ($|\eta|>3$) it is directed upwind. The principal source of error results from imperfect correction for the roll, pitch, and yaw of the plane. The peakedness coefficients c_{40},c_{22},c_{04} are such as to make the very large and very small slopes more probable than for a Gaussian distribution.

The effect of oil slicks covering an area of roughly one-fourth square mile is to reduce the mean square slope (regardless of direction) by a factor of two to three, to eliminate skewness, but to leave peakedness unchanged.

It is not difficult to show that gustiness leading to a standard deviation in wind speed of about one-third the mean wind speed could be responsible for the observed peakedness; nor is it impossible that systematic errors in the correction for background light may account for an appreciable part of the observed peakedness.

Comparison with Duntley

Duntley[11] has measured the surface slope components on Lake Winnipesaukee, N. H., by recording electrically the difference in immersion of pairs of thin vertical wires passing through the water surface. The wires were oriented to give simultaneous measurements of up/downwind and crosswind components. The separation between the wires was on different occasions 25 mm and 9 mm, consequently the measurements refer to the average value of slope over these distances.

Comparison of Duntley's results with ours show that (1) both investigations are consistent with a nearly Gaussian distribution of slopes; (2) both investigations indicate a linear increase of the mean square slope with wind speed; (3) the average value for the ratio σ_u^2/σ_c^2 is 1.5 for Duntley and 1.3 in our investigation; (4) the actual values for the mean square slopes are larger by a factor of 2.5 in Duntley's measurements than in ours. Possible explanations of (4) are the generation of short ripples by the wires themselves (fish line problem) as a consequence of the orbital movement of water past the wires and reflection of waves by the wire support mechanism.

[11] S. Q. Duntley, "The visibility of submerged objects." Part I, Optical Effects of Water Waves. Mass. Inst. Tech. Report, Dec. 15, 1950, on U. S. Office of Naval Research Report NO N5 ori-07831.

Comparison with Schooley

Schooley's method[12] consisted of measuring the high-lighted area on *resolved* photographs of the reflection of an artificial light source over a river. At medium wind speeds the agreement of the two sets of data is satisfactory, although the ratio σ_u^2/σ_c^2 is somewhat higher in Schooley's data. For the highest and lowest wind speeds, Schooley's slope values are significantly smaller than ours.

The larger ratio σ_u^2/σ_c^2 may well be the result of a smaller variability of wind direction. Schooley's photographs were made from a bridge over the Anacostia River, consequently the glitter pattern covered a very much smaller area in his photographs than in ours, and correspondingly would be expected to sample a smaller variability in wind.

The low values of the mean square slope components at very low winds in the river may easily be due to contamination of the river surface. At moderate winds, surface films would be swept away. Schooley's low values at high winds may be due to (1) the fetch on the river being so short that the mean square slope was still increasing downwind, and (2) the imperfect resolution of high-lighted areas on Schooley's photos. Visual inspection of sun-glitter indicates that the curvature distribution of the sea surface becomes peaked at greater and greater values the higher the wind speed. This results in the glitter spots becoming smaller at higher winds. Resolution of the photographic setup then sets a limit to the wind speed for which highlights can be resolved.

ACKNOWLEDGMENTS

We should like to express our appreciation to Captain Michael Sbarra, USAF, and his officers and crew, and to Steacy Hicks and Robert Huffer and the crew aboard the *Reverie* for their spirit of cooperation during all phases of this investigation. In Monterey, the Air Force plane was stationed at the Naval Auxiliary Air Station and the *Reverie* docked at the USCG Life Guard Station. We are indebted to both activities for their excellent cooperation. In Hawaii Mr. William Neilson of the Hawaii Aeronautic Commission was most helpful in arranging facilities for the plane. Here facilities for calibrating and processing the films were quickly set up in an abandoned hangar by Chief W. L. MacDonald, USN, and T/Sgt V. R. Cooke, USAF, who had joined the operation at NAAS, Monterey, and Hickam AF Base, Hawaii, respectively.

[12] A. H. Schooley, J. Opt. Soc. Am. 44, 37 (1954).